High Spectral Resolution Plasmonic Color Filters with Subwavelength Dimensions

Supplemental Information

Dagny Fleischman[1], Katherine T. Fountaine[2], Colton R. Bukowsky[1], Giulia Tagliabue[1], Luke A. Sweatlock[2], and Harry A. Atwater[1]

1. Thomas J. Watson Laboratories of Applied Physics, California Institute of Technology, Pasadena, CA 91125
2. Northrop Grumman NG Next, One Space Park, Redondo Beach, CA 90250, USA

16 pages, 8 figures, no tables

Contents:

Transmission Response

The single narrowband transmission peak of the optimized filter arises from the coupling of a large number of modes within the mirrored filter structure. The blue transmission curves in Supplemental Figure S1(a)-(c) is the champion filter identified by the numerical optimization method. The red, green, and violet curves are all deviations from the ideal geometry that illuminate the connection between the physical parameters and the optical response. The suppressed transmission in the red curve in Supplemental Figure S1(a) is due to a weak gap mode that prevents the modes supported by this filter from outcoupling into the far-field (a representative mode supported by this structure is shown in Supplemental Figure S2(b)). This gap mode, shown in Supplmental Figure S2(a) has a weaker electric field intensity than those of the two filters with higher transmission efficiency shown in Supplemental Figures S2 (c) and (g) (the green and violet curves in Supplemental Figure S1(b) and (c).

The primary source of the narrowband transmission is the thickness of the metal film spanning the region between the two mirrors. In Supplemental Figure S1(b), the physical parameters of the green curve filter are identical to that of the blue filter except that the green filter's film is twice the thickness of the blue filter. Increasing the thickness of the film pushes it outside the range of the skin depth of visible light, thereby preventing SPP modes from coupling across the surface of the film. The mode profiles verify that the supported modes only couple across the film in the thin film case. There is no evidence of cross-film coupling in the supported modes of the green curve filter (shown in Supplemental Figure S2(d) and (e)), but the thin film case clearly possesses cross-film coupling, as shown in Supplemental Figure S2(f).

By combining these conditions, a supported gap mode and cross-film coupling, it is possible to produce narrowband transmission features. The filter shown in the violet curve in Supplemental Figure S1(c) possesses a thin film and multiple narrow transmission features. Each of these features correspond to different supported modes in the structure. An example of a supported mode was determined for the peak at 688 nm and is shown in Supplemental Figure S2(h) which illustrates a cavity mode coupled to SPPs on the surfaces of the mirrors. This mode penetrates the thin film, as shown by both the non-zero field in the film and the weak SPPs supported on the film outside the cavity. The efficient gap mode shown in Supplemental Figure S2(g) allows for this

mode to out-couple for a transmission response. The dimensions for all filters described in Supplemental Figures S1 and S2 are listed in Supplemental Table S1. The mode profiles shown in Supplmental Figure S2 were all calculated using Lumerical's MODE solver for the four filters shown in Supplemental Figure S1.

Optimization Method

The process for optimizing the filter structure using the NOMAD algorithm and this FOM (main text, Eqn. 1) is illustrated in Supplemental Figure S3. All steps are performed automatically after the optimization process is initiated, using the optimization defaults unless indicated in Supplementary Table S2. In this method, the algorithm suggests a set of physical parameters for the filter. Lumerical Finite Difference Time Domain simulation package (FDTD), and eigenmode solver, then uses these parameters to perform a simulation to determine the filter's optical response. The resulting transmission spectrum of the filter is then analyzed by a custom peak-finding algorithm, which was developed to include both the maxima at the edges of a vector and plateaus, to make sure that all peak-like features would be properly identified and accounted for. Using the analyzed spectrum, the FOM is calculated, and used by NOMAD to suggest a new set of physical parameters. This process repeats until the convergence criteria is met.

Fabrication Method

The filters were fabricated using a novel metal imprinting process, shown in Supplemental Figure S4, which produces mirrors with straighter sidewalls than lift-off processing with the added benefit of producing extremely smooth metal structures. The initial steps shown in this process define SiO_2 structures that form the negative space around the metal mirrors using electron beam lithography. The fused silica chips are first sonicated in acetone before being rinsed in IPA. Next, a single layer of 950 A4 PMMA is spun at 1500 rpm for 1 minute and then baked for 5 minutes at 180°C. The fused silica substrate is electrically insulating, so a 5 nm Al film is thermally deposited on top of the resist to reduce charging during electron-beam patterning step. Electron-beam lithography is then used to write squares and rectangles that will eventually be the SiO_2 regions between the mirrors. After the patterning step, the Al film is etched away using 30% TMAH for 50 seconds, then the substrate is rinsed with DI water. The PMMA is then developed using MIBK:IPA 1:3 for 30 seconds and the substrate is rinsed in IPA.

Next, a 60 nm Cr film is deposited via electron beam evaporation at 0.6A/s in a chamber at pressure $5.3x10^{-7}$ torr. The PMMA and unwanted Cr are then removed via lift off using Remover PG for 5 minutes and occasional sonication. The remaining Cr film is used as an etch mask during a 1:54 m:s ICP etch in C_4F_8/O_2 that defines 600 nm tall SiO_2 pillars. The Cr etch mask is then removed by a 20 minute soak in Cr-7S etchant solution.

Once the Cr is removed, a 1 nm layer of HfO_2 is deposited via an 8 cycle deposition in an ALD. Next, 2 μm of Ag is deposited on top of the sample. The sample is rotated to try to ensure as conformal a deposition as possible. The height of the SiO_2 pillars prevents completely infilling of the regions between the pillars. To create Ag mirrors that are flush to the SiO_2 pillars, a wafer bonder was used to press a dummy chip of thermal SiO_2 on Si onto the Ag film. The stack is held at 1500 torr and 175°C overnight, to allow the Ag to infill into the voids near the SiO_2 pillar and the top of the film to reach the smoothness of the SiO_2 on Si dummy chip. This process also considerably reduces the surface roughness of metal films, decreasing the RMS roughness of the as-deposited film from 5.58 nm down to 0.55 nm, as shown by the AFM scans in Supplemental Figure S5.

After the Ag is pressed around the SiO_2 pillar to form the mirrors, there is a 1.48 μm thick film of Ag on top of the pillar that must be milled to the final 50 nm thickness. An Ar mill in an ICP plasma etch system was used to remove the excess Ag. Different grains in Ag etch at different rates, so the forward power was increased to its maximum value of 300W to make the etch as physical as possible. The sample was milled for 6 minutes at a rate of 205 nm/min yielding a 255 nm thick film. The etch was stopped before the final 50 nm was reached to do a second pressing step to smooth out any thickness variations due to the grain texturing. The Ag film is then etched for another 32 seconds to bring the final thickness to 50 nm.

These 50 nm Ag films are relatively transparent to back scattered electrons generated by a 30 kV and 100 nA electron beam. This transparency was used to align the slit between the mirrors during the FIB process. While a 30 kV Ga beam does not generate enough back scattered electrons for

visibility, by aligning the electron and ion beams to a coincident point, the proper position can be observed using the electron beam and then milled using a low current ion beam.

Once the slits were milled, 1.4 μm of SiO_2 were deposited in a PECVD using SiH_4/Ar. The films deposited in the PECVD used are not conformal at the edges of chips, so to prevent the sample from oxidizing, an additional 8 nm of Al_2O_3 was deposited in an ALD on top of the SiO_2 film to ensure the sample was completely encapsulated. To prevent the H_2O precursor from oxidizing the edges during the ALD processing, the sample was first coated with extra-long pulses of the Al_2O_3 precursor and then subject to 40 cycles of 50°C Al_2O_3 depositions before depositing the final 4nm at 150°C[1]. Cross-sections of a filter prior to milling and a completed filter are shown in Figure S4(a) and (b) of the main text.

While the fabrication process used to make the measured filters uses serial patterning systems such as electron beam lithography, focused ion milling, and makes unconventional use of a wafer bonder, these filters can be fabricated in a nanofabrication foundry environment. The electron beam lithography and focused ion milling steps can also be replaced by a two-step aligned photolithography process that defines two SiO_2 pillars. During the first photolithography step, a small pillar that will become the slit can be etched onto an SiO_2 film. In the second photolithography process, a larger pillar can be defined under the small pillar to become the spacing between the mirrors. After the metal is deposited on the stacked pillars, a chemical mechanical polishing system can be used to thin the metal down and smooth it flat, leaving the top of the slit exposed, and finishing the filter with the final SiO_2 coating step.

Measurement Set-up and Analysis

The custom-built optical transmission measurement set-ups used in this work are shown schematically in Supplemental Figure S6. In this configuration, a beam supplied by a NKT SuperK Extreme white laser was monochromated with variable slit width to give a constant bandpass of 2nm, collimated, expanded by two 90 degree off-axis parabolic mirrors, and finally focused onto the sample with a long working distance, low-NA objective (Mitutoyo Plan Apo 50X,

Tube Length 200mm, NA=0.55). Using a CMOS (IDS UI-1460SE) camera we characterized experimentally the beam shape at the focal plane and verified it had a FWHM of ~2nm.

A calibrated Si photodetector (Newport 818-ST2-UV) was used to measure the power transmitted through the filter, as well as the reference 5um aperture. During all measurements the beam was sampled with a glass slide and measured with a Si reference photodiode for simultaneous recording of the beam photocurrent, allowing correction of any fluctuations in the laser power between a normalization measurement and measurement of the samples. A chopper, typically at a frequency of 95Hz, was used to modulate the incident beam, and provide a reference frequency to two Stanford Research Systems SR840 lock-in amplifiers. An external, low-noise current-to-voltage transimpedance amplifier was used to feed both photodiode signals to the respective lock-in amplifier. The lock-in amplifiers were used to filter the modulated signal from other potential noise signals in the photodiode responses.

In order to attenuate background signal as much as possible, the optical transmission setup described above was further modified into a transmission confocal microscopy configuration. The same monochromatic and collimated beam was redirected 180° via mirrors to enter the objective passing through its focal point. A second objective (Mitutoyo Plan Apo 2X, Tube Length 200mm, NA=0.05) focused and collimated the beam at the focal spot. The back side of the filter being measured was placed at the focal point of the high N.A. objective, creating a transfer function of the transmitted light. This collimated beam was refocused with a 100mm focal length plano-convex lens to form an image of the transmitted light. A 50μm pinhole was placed in this image plane. The portion of the image transmitted by the pinhole was controlled by translating the sample, rather than the pin-hole in the image plane. Due to the tube length being larger than 200mm, the actual magnification of this image was about 62x. The equivalent diameter of the aperture with respect to the magnified image was about 5μm as measured by the CMOS camera. A low dark current photodiode was used behind this pinhole to measure the transmitted photocurrent through the lock-in amplifier system. The imaging objective was calibrated for chromatic focal shifts and the position of the objective was adjusted with sub-micrometer steps to further reduce chromatic aberrations. Peak normalized signal-to-noise (SNR) plots were created using this method because it significantly increased spatial signal contrast and greatly reduced the background spectrum such that sub-percent peaks could be detected without a loss in SNR. The

normalization spectrum for each filter was measured on an area of the fused silica superstrate where no Ag film existed, which accounted for the reflection of the superstrate.

Angle Dependence of Mirrored Filters

The transmitted peak position of the mirrored filters is independent of incident angle. As shown in Supplemental Figure S8, when an incident plane wave is injected at angles ranging from 0 to 40°, the transmitted peak position does not shift. The transmission efficiency is reduced with increasing angle, because as the incident angle gets steeper, progressively more of the light is incident on the perfectly matched layer (PML) boundaries surrounding the simulation region instead of onto the filter itself, leading to an effective reduction of the apparent transmission. The angle insensitivity of the filters was further confirmed by simulating the transmission response of the filters when illuminated with Gaussian beams with varying numerical apertures (NAs). As the NA increased, the transmission efficiency also increased, because more of the incident light was focused into the region between the two mirrors in the filter. The angle insensitivity of these filters prevented any detrimental effects from the increased angular distribution of the incident light from the higher NA Gaussians.

Figures

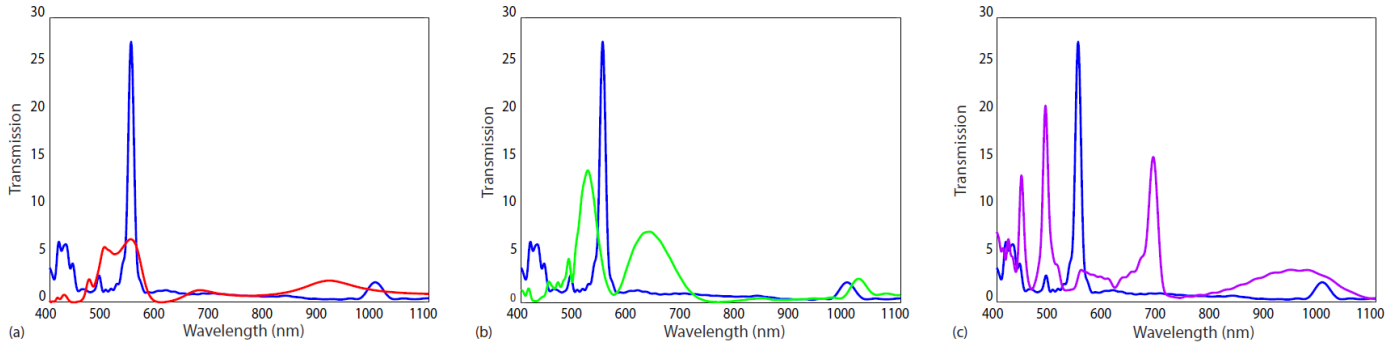

Supplemental Figure S1: (a) comparison between a champion filter (blue) and a filter with reduced transmission (red). The red curve filter possesses a much smaller mirror spacing than the champion filter and a thicker film, which prevent efficient out-coupling of the supported modes (b) comparison between a champion filter (blue) and a filter (green) with the same physical parameters except for a thicker film, indicating that the thickness of the film between the mirrors plays a very large role in the narrow transmission bandwidth. (c) comparison between a chamption filter (blue) and a filter (violet) with multiple resonances that produce narrow transmission features. The physical parameters of all filters shown are listed in Supplementary Table S1. Representative mode profiles for each of these filters are shown in Supplemental Figure S2

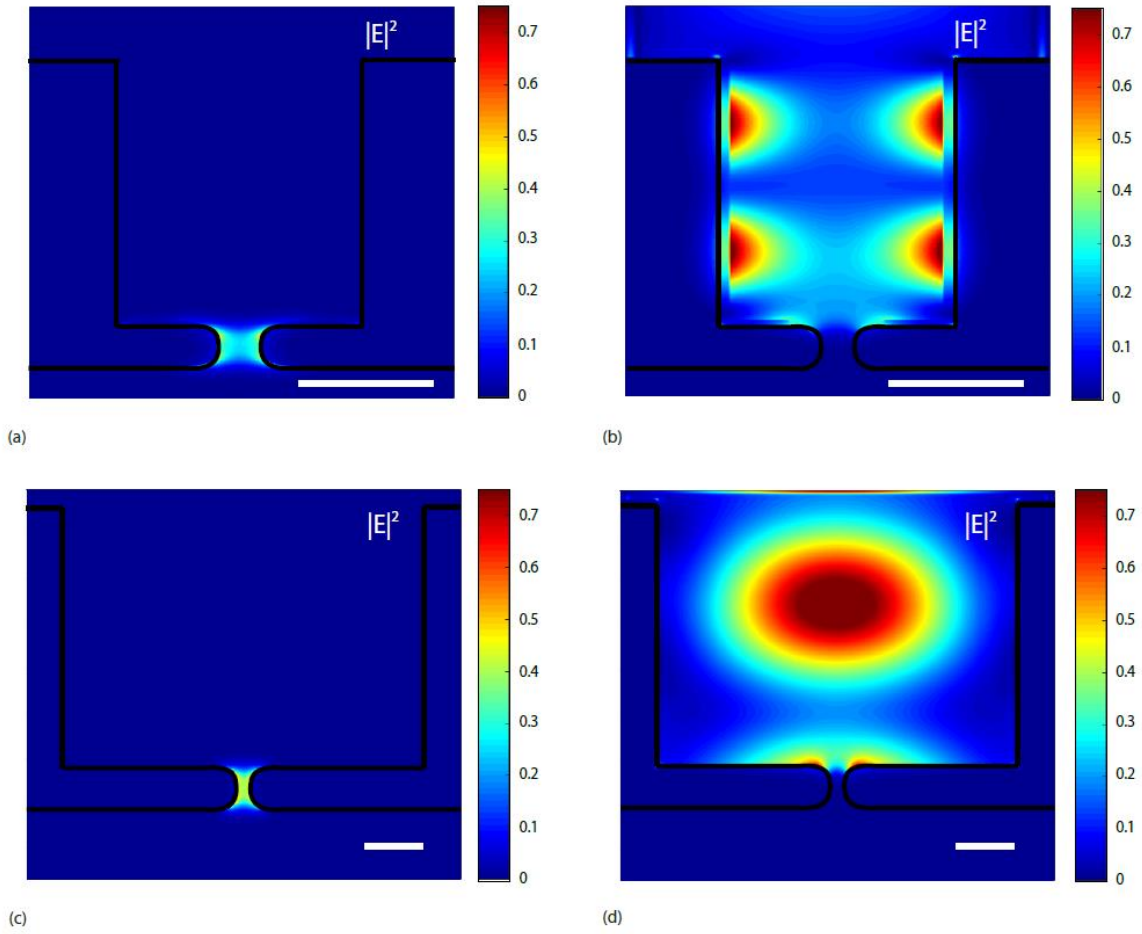
|E|²
0.7
0.6
0.5
0.4
0.3
0.2
0.1
0
(a)
(b)
(c)
(d)

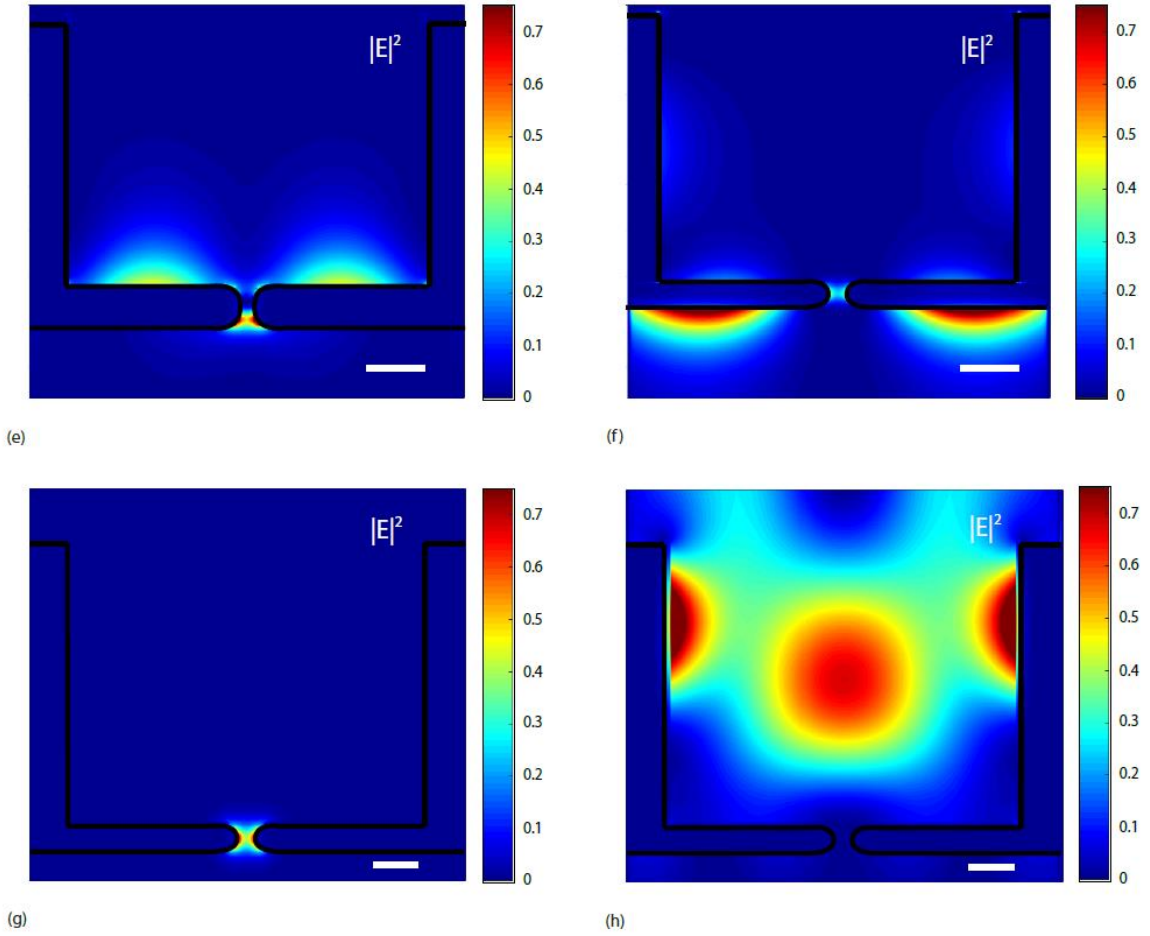

Supplemental Figure S2: (a) and (b) are electric field intensity mode profiles for Supplmental Figure S1(a) red curve filter calculated at 547 nm. The relatively weak gap mode in (a) prevents efficient outcoupling of the mode shown in (b), which leads to this filter's low transmission intensity. (c)-(e) are mode profiles for the green curve filter shown in Supplemental Figure S1(b) calculated at 614 nm. The more efficient gap mode allows for a higher out-coupling of the cavity mode shown in (d) and the SPP shown in (e), which is reflected in the transmission curve shown in Supplemental Figure S1(b). The transmission features are still relatively broad, but by reducing the thickness of the metal film, while holding the rest of the physical parameters of this fixed, the transmission peak can be narrowed. A mode profile calculated at the filter transmission peak at 554 nm is shown in (f) where it is possible to see electric field intensity spanning the thin film, indicating that the top and bottom surface SPPs are coupled and interacting, leading to a much reduced bandpass for this filter relative to the thick film case. (g) and (h) are the mode profiles calculated for the violet curve shown in Supplemental Figure S1(c) at 688 nm, which posseses multiple narrow transmission features. (g) indicates, as expected, that the gap mode is efficient enough to allow for modes to couple out of the filter. The profile shown in (h) indicates that the interacting cavity and SPP modes also couple to the SPPs on the far side of the thin film, which lead to the sharp transmission features present in this filters spectral response.

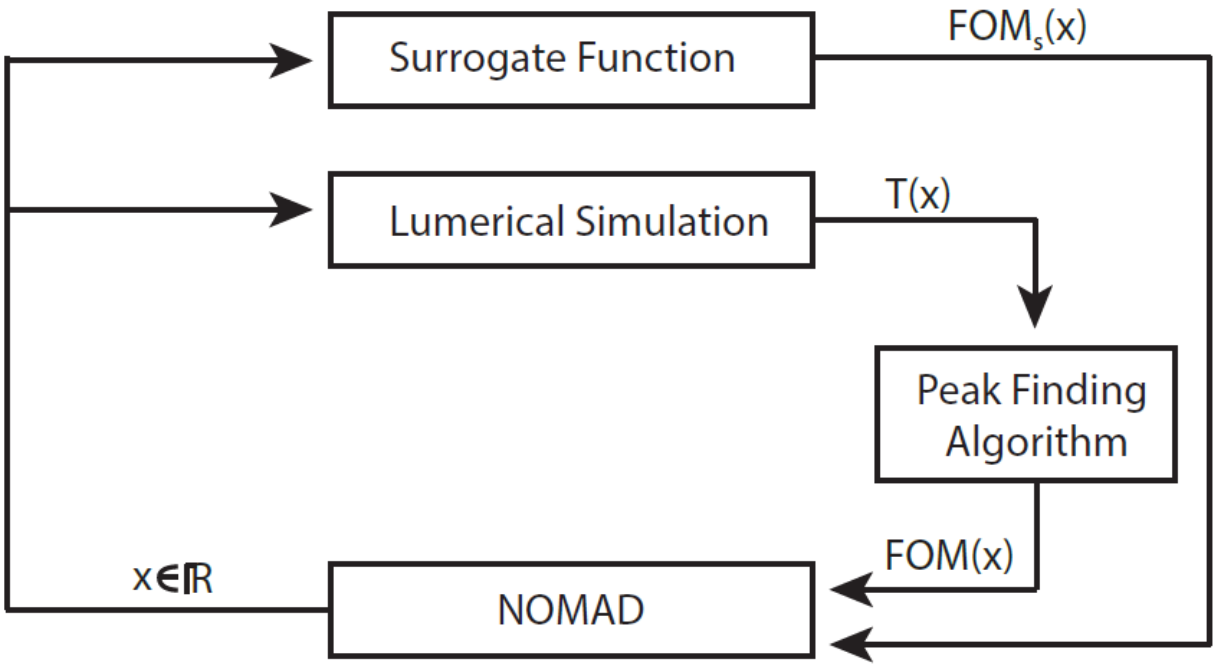

Supplemental Figure S3: The components of the filter optimization process. The Nonlinear Mesh Adaptive Direct Search algorithm (NOMAD) determines the parameters probed to find the optimal solution. Once the physical parameters (x) are selected, they will either be evaluated by the surrogate function or a Lumerical calculation, which return the FOM to NOMAD. For each Lumerical calculation, the transmission response is analyzed by the peak finding algorithm to determine the FOM, which can then be used by NOMAD

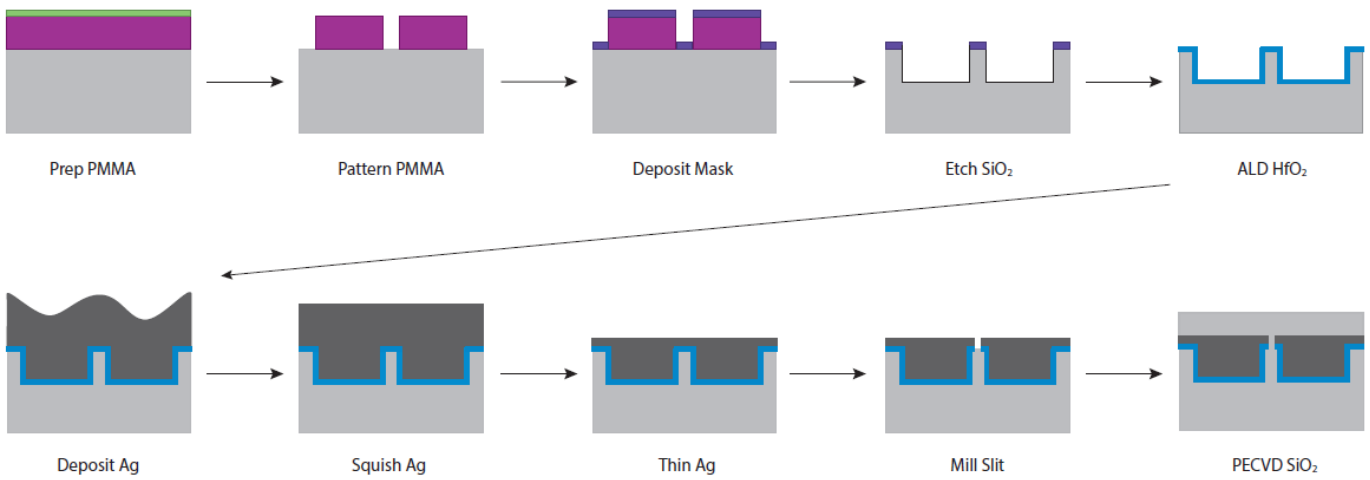

Supplemental Figure S4: The process flow for fabricating mirrored filters. First the region between the mirrors is defined in a fused silica substrate using a pattern defined by electron-beam lithography that is subsequently dry etched. Next a thick layer of Ag is deposited and pressed into the etched regions to form the mirrors. The Ag is then thinned to the final thickness of the thing film and the slit is milled before SiO2 is deposited on the top surface to encapsulate the Ag.

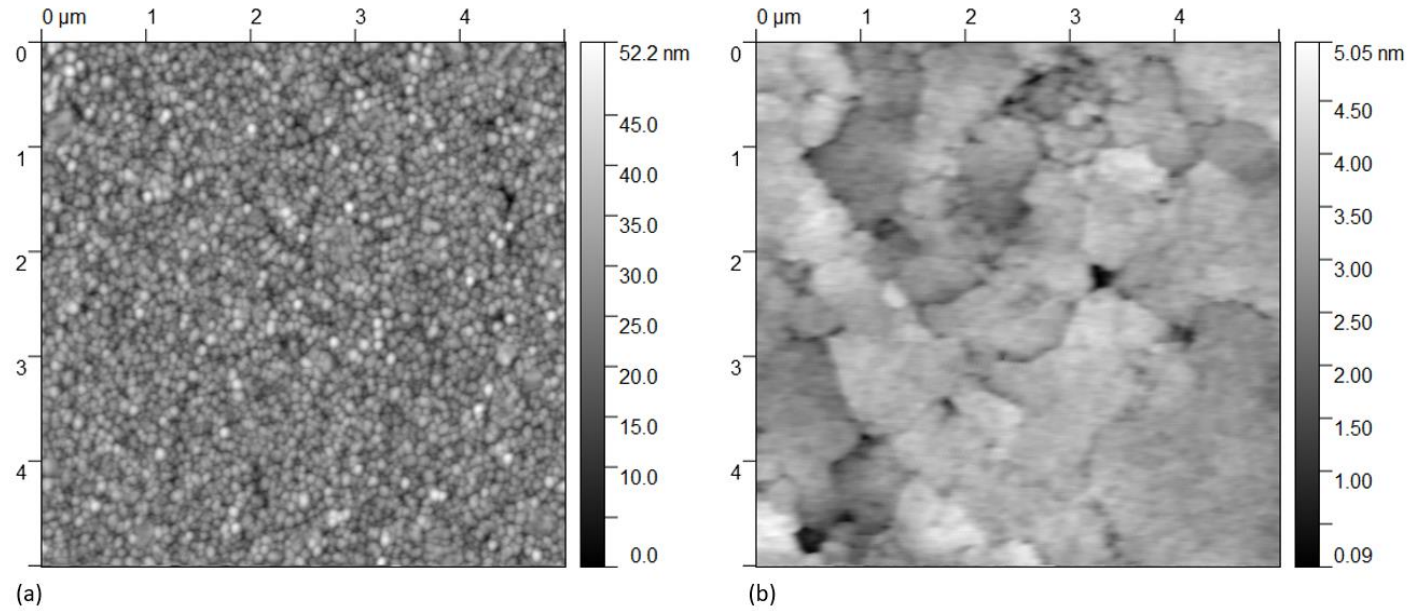

Supplemental Figure S5: AFM scans illustrating the smoothing effect of the wafer bonder pressing process. (a) An electron beam evaporated Ag film that was not pressed. The RMS roughness is 5.58 nm (b) An Ag film deposited in the same conditions that was then pressed at 1400 torr and held at 100 °C for 6 hours that has an RMS of 0.55 nm

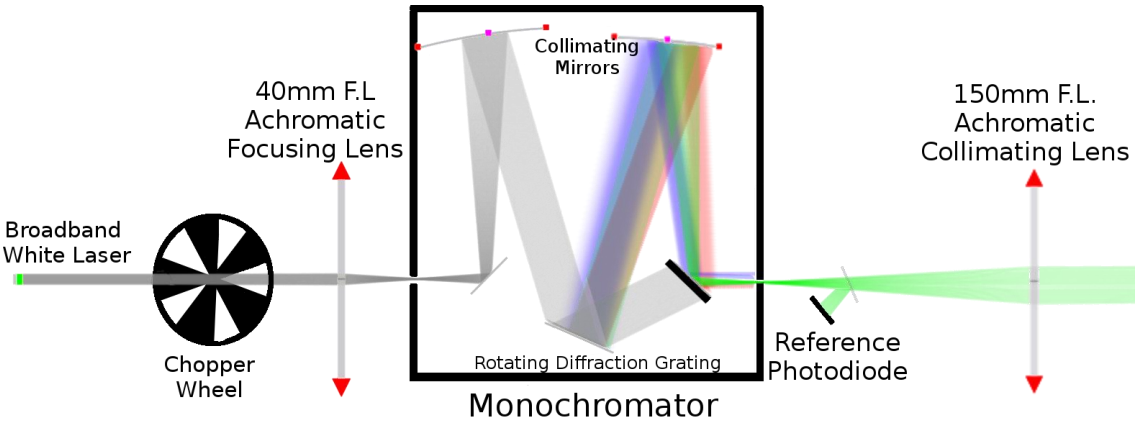
Collimating
Mirrors
40mm F.L
Achromatic
Focusing Lens
150mm F.L.
Achromatic
Collimating Lens
Broadband
White Laser
Chopper
Wheel
Rotating Diffraction Grating
Reference
Photodiode
Monochromator

(a)

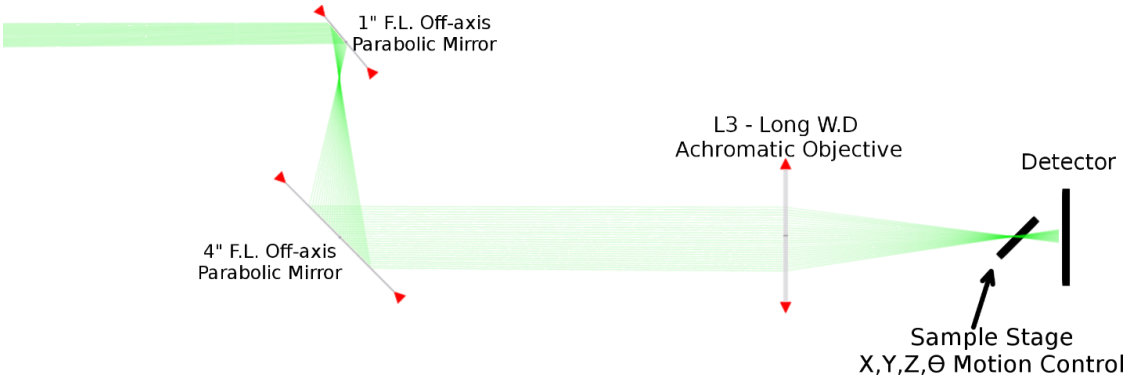
1" F.L. Off-axis
Parabolic Mirror
L3 - Long W.D
Achromatic Objective
Detector
4" F.L. Off-axis
Parabolic Mirror
Sample Stage
X,Y,Z,Θ Motion Control

(b)

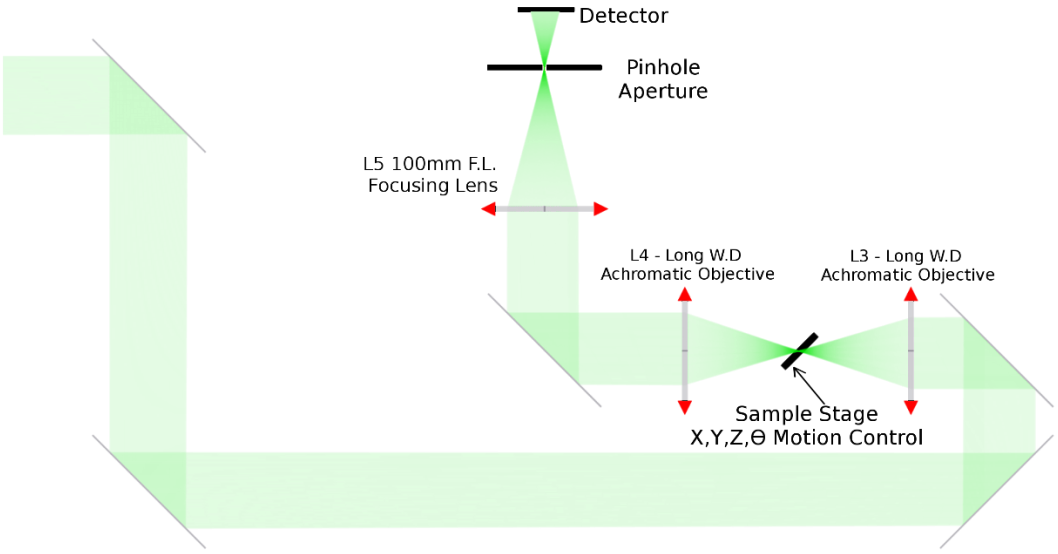
Detector
Pinhole
Aperture
L5 100mm F.L.
Focusing Lens
L4 - Long W.D
Achromatic Objective
L3 - Long W.D
Achromatic Objective
Sample Stage
X,Y,Z,Θ Motion Control

(c)

Supplemental Figure S6 (a) Schematic of the optical set-up depicting the monochromation and collimation of the light beam and the collection of the reference signal (b) Schematic of the focusing of light onto the sample and the collection of the transmitted signal with a Si Photodetector. (c) Schematic of the confocal transmission microscopy configuration. The ultracompact Ag filter transmits light into the high N.A. objective and it is imaged onto a pinhole aperture which selects a 5um diameter portion of the image signal.

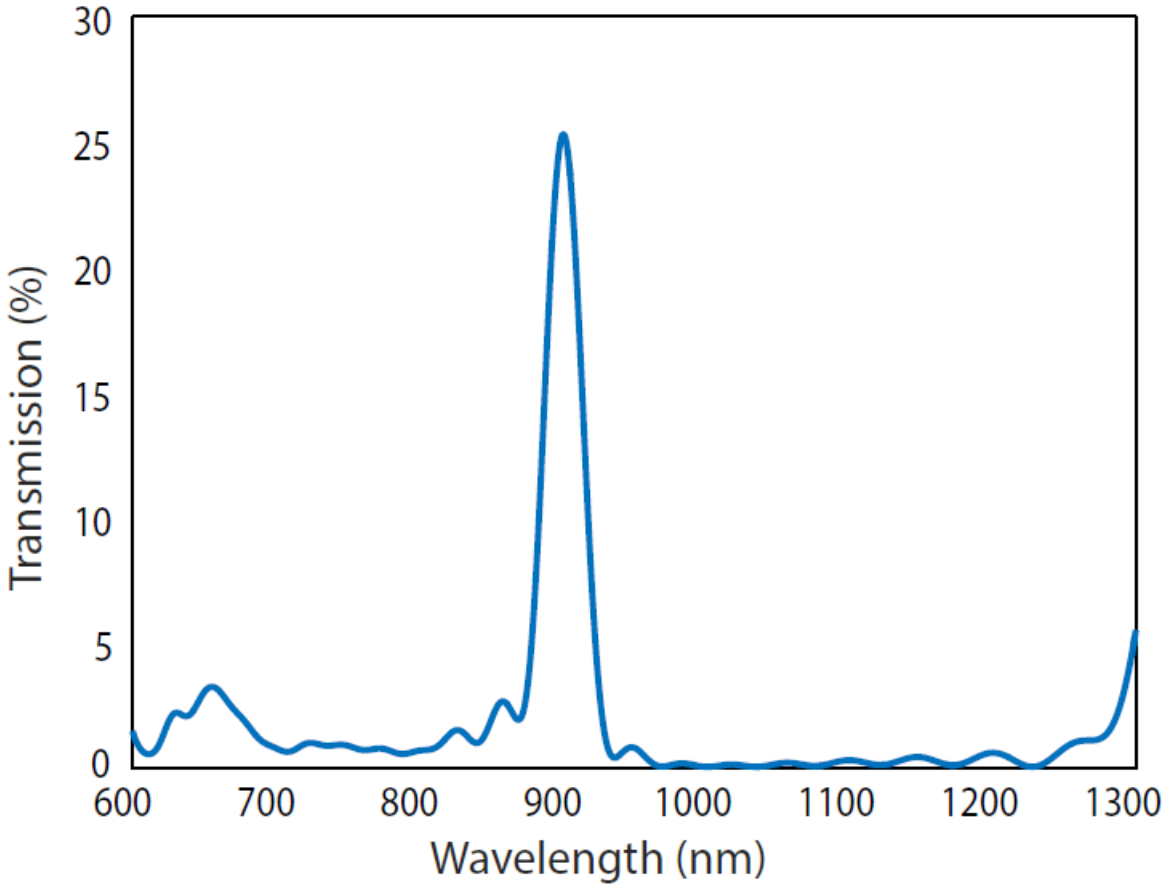

Supplemental Figure S7: A sample simulated transmission response for a near IR mirrored color filter that has Cu metal components

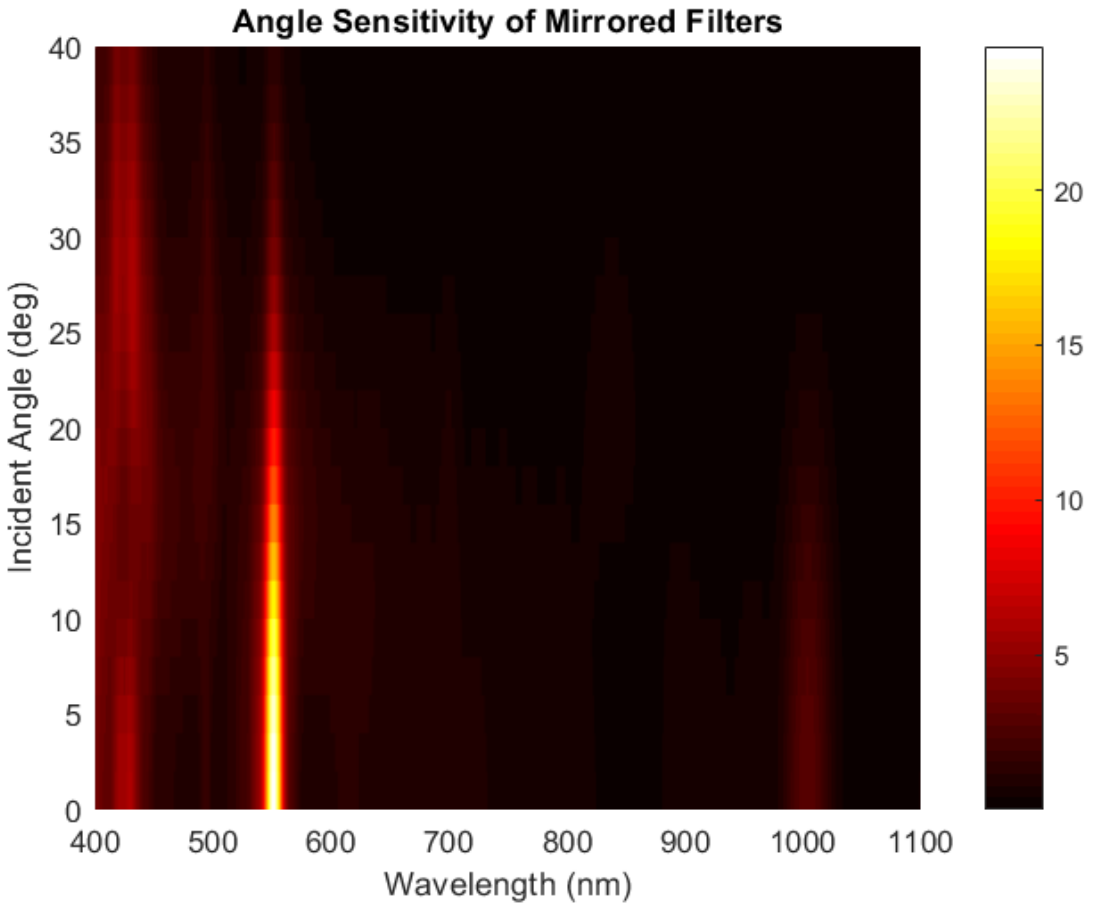

Supplemental Figure S8: The angle dependence of a linear mirrored filter illuminated with a plane wave with angle of incidence ranging from 0 to 40°

Tables

Supplementary Table S1

Curve	Blue	Red	Magenta	Green
Mirror Spacing	620	180	800	620
Mirror Height	598	598	598	598
Film Thickness	48	84	48	96
Gap Width	31	44	44	31
Oxide Thickness	1	12	12	1

Supplementary Table S1: Physical parameters for the filters with responses plotted in Supplemental Figure S1. All dimensions are in nm.

Supplementary Table S2

Setting	Filter Optimization	Default
Surrogate Sample Points	500	20
Minimum Mesh Size	1e-3	1e-4
Initial Mesh Size	1	0.1
Surrogate Minimum Mesh Size	0.05	0.01

Supplementary Table S2: Settings where the NOMAD defaults vary from those used during the Mirrored Filter Optimization

References

1. Wood, J. D. *et al.* Effective passivation of exfoliated black phosphorus transistors against ambient degradation. *Nano Lett.* **14,** 6964–6970 (2014).